Zakharova, O., Hainzl, S., Bach, C. (2013): Seismic moment ratio of aftershocks with respect to main shocks. - *Journal of Geophysical Research*, *118*, 11, p. 5856-5864.

DOI: http://doi.org/10.1002/2013JB010191

Seismic moment ratio of aftershocks with respect to main shocks

O. Zakharova,[1] S. Hainzl,[1] and C. Bach[1]

Received 13 March 2013; revised 24 September 2013; accepted 23 October 2013; published 15 November 2013.

[1] The empirical Båth's law indicates that the earthquake process is self-similar and provides an opportunity to estimate the magnitude of the largest aftershock subsequent to a main shock. However, the analysis of this relation is limited to a small magnitude range and also depends on the aftershock selection rules. As an alternative, we analyze, in this paper, the cumulative seismic moment of aftershocks relative to the main shock moment, because (i) it is a physical quantity that does not only take the largest aftershock into account; (ii) background activity can be considered and as a result estimations are less affected by selection rules; and (iii) the effects of the catalog cut-off magnitude can be corrected, what leads to larger magnitude range for the analysis. We analyze the global preliminary determination of epicenters U.S. Geological Society catalog (combined with centroid moment tensor focal mechanisms) and find that the seismic moment release of aftershocks is on average approximately 5% of the main shock seismic moment. We show that the results can be well fitted by simulations of the Epidemic Type Aftershock Sequence model. In particular, we test whether simulations constrained by predictions of the static stress-triggering model, proposing a break of self-similarity due to the finite seismogenic width, are in agreement with observations. Our analysis shows that the observed dependency on the main shock magnitude as well as systematic variations with the main shock fault plane solution can be both explained by the constraints based on the static stress triggering.

Citation: Zakharova, O., S. Hainzl, and C. Bach (2013), Seismic moment ratio of aftershocks with respect to main shocks, *J. Geophys. Res. Solid Earth*, *118*, 5856–5864, doi:10.1002/2013JB010191.

1. Introduction

[2] It is well known that earthquakes are strongly correlated in time and space. A good example of such a correlation is aftershock triggering by main shock. The event dependence can be partly explained by stress changes and structural heterogeneity of the crust [*Stein*, 1999]. In the present work, we focus on the dependency between the magnitude of main shocks and their aftershocks and aftershock cascading triggering. One important empirical feature of aftershock sequences is the Båth's law [*Båth*, 1965]. This law states that the magnitude difference Δm between a main shock and its largest aftershock does not depend on the size of the mother event; although Δm varies a little with the region of interest [*Felzer et al.*, 2002; *Console et al.*, 2003] and is different in strike-slip and reverse/normal faulting environments [*Tahir et al.*, 2012]. According to the Båth's law, this magnitude difference is in general equal to 1.2.

[3] The observation that Δm is constant indicates that the total number of aftershocks scales with $\sim 10^{bm_m}$ as a function of the main shock magnitude m_m, where b is the b value of the Gutenberg-Richter law. This is equivalent to a scaling with the seismic moment M_m of the main shock according to $\sim M_m^{(2/3)b}$. In contrast, a break of the scaling is expected in physical models of earthquake triggering due to the limited size of the seismogenic depth (change of material properties with depth from brittle crust to viscous-elastic mantel). In particular, recent results of a clock advance model based on the static stress interaction suggest that the productivity of small main shocks scales with $\sim M_m$, while that for larger events scales approximately according to $\sim M_m^{2/3}$ [*Hainzl et al.*, 2010]. Consequently, the empirical observation of the Båth's law seems to disprove the static stress-triggering model.

[4] However, it has to be taken into account that the quantity Δm has a rather limited resolution. In particular, it can be only analyzed in the magnitude range $m_m \geq m_c + 2$, where m_c represents the completeness magnitude of the analyzed catalog [*Helmstetter and Sornette*, 2003]. Furthermore, the result is biased by cluster selection rules because of missed aftershocks or misinterpretation of independent background events as aftershocks. To minimize these problems, we focus in this study on the ratio R between the seismic moment released by aftershocks and by the main shock. As shown in the following, this value, based on observations, can be corrected for background events and undetected smaller magnitude events. This enables the analysis of observed seismicity and its comparison with earthquake models in a significantly larger magnitude range.

[1]GFZ German Research Centre for Geosciences, Potsdam, Germany.

Corresponding author: O. Zakharova, GFZ German Research Centre for Geosciences, Telegrafenberg, 14473 Potsdam, Germany. (olgaza@gfz-potsdam.de)

2169-9313/13/10.1002/2013JB010191

[5] We compare observations with simulations of the Epidemic Type Aftershock Sequence (ETAS) model [*Ogata*, 1988]; in particular, also to a model version in which the aftershock-trigger potential is constrained by the results of the scaling aspect of the static stress-triggering model. After introducing the applied methodologies in section 2, we test in section 3 several predictions of the restricted ETAS model, in particular, the value of Δm and R as a function of the main shock magnitude as well as their dependency on the focal mechanism. Our findings are finally discussed and summarized in sections 4 and 5.

2. Methods

[6] In the present work, we focus on two values of earthquake sequences—the magnitude difference between the main shock and its largest aftershock

$$\Delta m = m_m - m_{a,\max} \tag{1}$$

and the ratio R between the seismic moment released by all aftershocks and the main shock. For the latter, we use the formula $M(m) = 10^{9.1+1.5m}$ [*Hanks and Kanamori*, 1979] and calculate the seismic moment released by the main shock $M_m = M(m_m)$, before-main shock activity $M_f = \sum_{i:t_i<t_m} M(m_i)$ (all events which occurred before the main shock) and after-main shock activity $M_a = \sum_{i:t_i>t_m} M(m_i)$ (all events in the sequence after the main shock), where t_m is the main shock occurrence time.

[7] While the presence of the background events cannot be directly considered in the Δm-value, the influence of the background activity can be taken into account by calculating the difference $M_a - M_f$. However, it should be noted that M_f also includes potential foreshocks. Hence, the term $M_a - M_f$ can be interpreted as the excess of the after-main shock seismic moment release relative to the before-main shock release. For the estimation of the before- and after-main shock seismic moment release, we use time windows $[-T, 0]$ and $[0, T]$, respectively. Thus, the calculated ratio between triggered and main shock seismic moment release is

$$R = \frac{M_a - M_f}{M_m}. \tag{2}$$

However, the resulting R value is an underestimation of the true value of the seismic moment ratio, because of missed events with magnitudes below the detection threshold m_c. This means that the seismic moments of events with magnitudes $m < m_c$ are not considered in equation (2), but this can be corrected for a given b value. Let us assume that the frequency-magnitude distribution of foreshocks and aftershocks is given by the Gutenberg-Richter law, 10^{a-bm}, where only the a value is different between the foreshock and aftershock distribution. The ratio between the total seismic moment release and the observed one for foreshocks and aftershocks in the magnitude range $[m_c, m_m]$ is given by

$$C(m_m) = \frac{\int_{-\infty}^{m_m} 10^{9.1+1.5m} 10^{a-bm} \mathrm{d}m}{\int_{m_c}^{m_m} 10^{9.1+1.5m} 10^{a-bm} \mathrm{d}m} = \frac{1}{(1 - 10^{-(1.5-b)(m_m-m_c)})} \tag{3}$$

Because this correction factor is the same for foreshocks and aftershocks, the corrected unbiased value of the seismic moment release ratio is consequently $R_{\mathrm{corr}}(m_m) = C(m_m)R(m_m)$.

[8] Based on the seismic moment ratio, we are able to calculate an equivalent magnitude difference

$$\Delta m_{\mathrm{eff}} = -\frac{\log_{10}(R_{\mathrm{corr}})}{1.5} = m_m - m_{a,\mathrm{eff}} \tag{4}$$

with the effective magnitude for the triggered activity

$$m_{a,\mathrm{eff}} = \frac{\log_{10}[(M_a - M_f)C(m_m)] - 9.1}{1.5}. \tag{5}$$

The effective magnitude can be seen as a replacement of the magnitude $m_{a,\max}$ in the Båth's law ($\Delta m = m_m - m_{a,\max}$), which takes the cumulative seismic moment release of all aftershocks into account. To avoid the situation, when $R = 0$, we calculate the effective magnitude difference Δm_{eff} from the average of R over all clusters. We analyze these quantities (Δm, R, and Δm_{eff}) for earthquake sequences in observational global data sets and ETAS simulations, which are both introduced in the following subsections.

2.1. Observational Data

[9] We analyze the global U.S. Geological Society preliminary determination of epicenters (PDE) catalog in combination with the catalog of centroid moment tensor (CMT) focal solutions. While the magnitudes are taken using the PDE catalog, the fault plane solutions are added from the CMT data set for that cases in which events could be matched. For the analyzed time period between 1973 and 2011, we used a cutoff magnitude of $m_c = 5.0$ and only consider shallow events with a depth less than 50 km. The magnitude of completeness is equal to the cutoff magnitude.

[10] To separate seismic events into main shocks (independent earthquakes) and their respective foreshocks/aftershocks (dependent earthquakes), no unique procedure exists and several alternative cluster selection procedures have been introduced in the past. A summary of the most prominent clustering procedures is given by *van Stiphout et al.* [2012]. In our work, we follow the window-based procedure of *Tahir et al.* [2012] for cluster selection. According to this, an earthquake with magnitude m is defined as a main shock, if it is the largest earthquake within the time period $[-T, +T]$ and a distance range $D(m)$. The spatial window is set to be a multiple of the rupture length, i.e., $D(m) = \kappa L(m)$, where $L(m) = 10^{-2.44+0.59m}$ is a subsurface rupture length for all types of focal mechanisms in kilometers [*Wells and Coppersmith*, 1994] and κ is a constant variable coefficient. The time interval for our subsequent analysis is $T = 1$ year, although typical aftershock sequences are longer. However, longer time intervals would lead to an enlarged contamination by background activity. Using the fixed time span of 1 year, we account for the same fraction of aftershocks independently of the main shock magnitude. According to the Omori-Utsu law [*Utsu et al.*, 1995], this fraction of aftershocks $f_a = N_{\mathrm{after}}(T = 1\mathrm{year})/N_{\mathrm{all}}(T_{\mathrm{all}})$ is, e.g., equal to 0.97 and 0.95 for $p = 1.2$ and the total aftershock duration of $T_{\mathrm{all}} = 10$ years and $T_{\mathrm{all}} = 100$ years, respectively. The parameter κ is set in the range $[1, 5]$ in accordance with general observations of aftershock occurrences. The lower

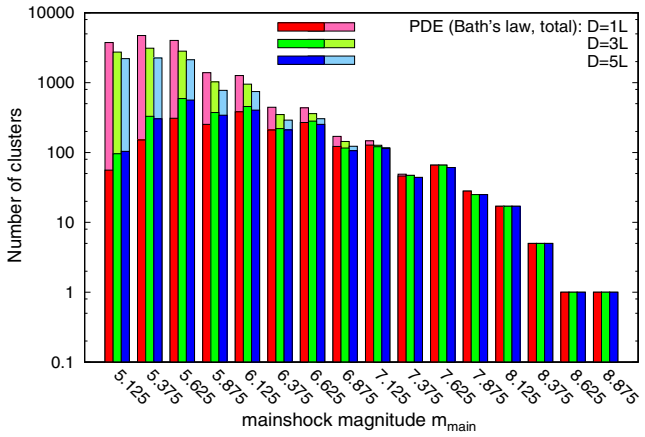

Figure 1. The distribution of cluster numbers (PDE catalog) with respect to the magnitude of the main shock and selection criteria. Each bar is related to the number of clusters, which are used for the calculations of the effective magnitude and seismic moment ratio. Dark colored bars indicate the number of main shocks used for the Båth's law estimation and include at least one aftershock. The magnitude value indicates the mean value of each bin with width 0.25.

limit for κ can be defined according to the minimum area of the aftershock distribution, i.e., the radius of space window is equal to one rupture length. The upper boundary for the rupture length is less clear, because remote aftershock triggering is known to occur very far away and these events will be missed for smaller values of κ. However, increasing κ will also increase the number of independent background events that are wrongly identified as foreshocks or aftershocks. That is why we use different radii in the range between one and five rupture lengths in our cluster selection procedure and compare the corresponding results.

[11] Not all the data can be used for the analysis of the Båth's law because the calculation of Δm requires at least one aftershock in a cluster. To illustrate the number of clusters available for the different calculations, we present a histogram of the number of clusters with respect to the main shock magnitude in Figure 1. Dark colors indicate the number of main shocks, which can be utilized for the Δm value estimation, while the light colors show the number which can be used for all other calculations. We provide histograms for all applied spatial windows of the cluster selection. For magnitudes larger than 7.5, the number of clusters is the same for all types of analyses, while for smaller magnitudes, less than 10% of the clusters can be used for the calculations related to the Båth's law. In addition, Figure 2 shows the histograms for the number of clusters that we obtained after combining the PDE catalog with CMT solutions as a function of the main shock rake and time, respectively.

2.2. ETAS Simulations

[12] For comparison with the observed data, we additionally analyze Monte-Carlo simulations of the Epidemic Type Aftershock Sequence (ETAS), which is nowadays one of the standard models for describing the first-order statistical features of earthquake clustering [*Zhuang et al.*, 2012]. This statistical model is constructed based on a number of well-established empirical laws. The temporal correlations are described by the Omori-Utsu law, which states that the rate of triggered aftershocks decays with time t relative to the main shock according to [*Utsu et al.*, 1995]

$$n(t) = \frac{K}{(t+c)^p}, \tag{6}$$

where K, c, and p are constant parameters. Furthermore, the aftershock productivity parameter K depends exponentially on the main shock magnitude, $K \sim 10^{\alpha m_m}$. However, while the functional form is well established, the estimations of the parameter α vary largely between different estimation procedures [*Hainzl and Marsan*, 2008].

[13] The ETAS model introduced by [*Ogata*, 1988] is based on these empirical relations and assumes that every earthquake has a potential to trigger its own aftershocks. There is no preestablished difference between main shocks, foreshocks, and aftershocks in the ETAS model. All events in the ETAS model are equivalent, and events with smaller magnitudes can also generate earthquakes with larger

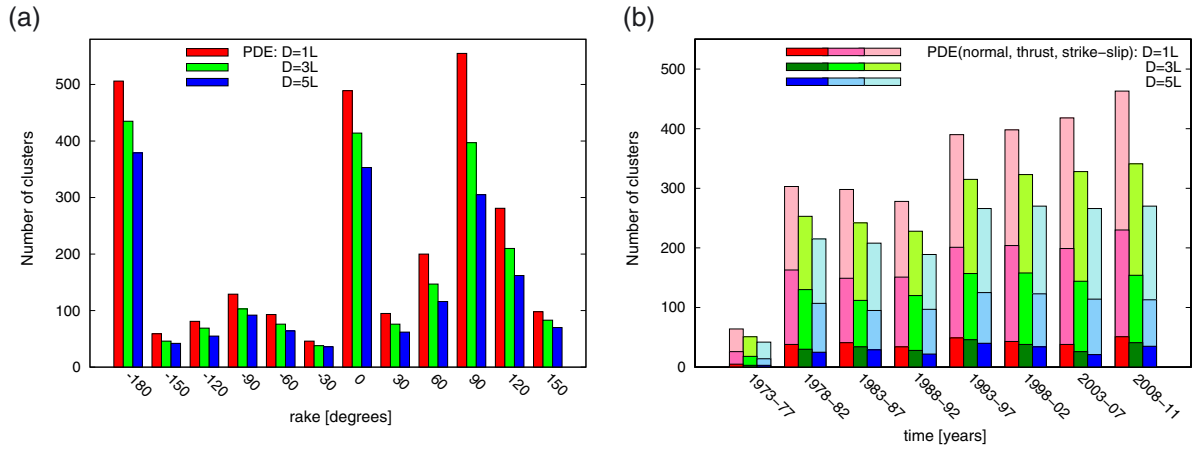

Figure 2. Histograms of the number of clusters (PDE + CMT catalog) as a function of (a) the rake of the main shock and (b) the occurrence time for different selection criteria. In Figure 2b, the different color shadings refer to the different rupture styles.

magnitudes. Earthquakes are only retrospectively classified as main shocks, foreshocks, and aftershocks by their time occurrence in the cluster. As a consequence of the aforementioned, the earthquake rate λ at time t is described in the ETAS model by

$$\lambda(t) = \mu + \sum_{i:t_i<t} g(m_i) f(t-t_i) = \mu + \sum_{i:t_i<t} K_0\, 10^{\alpha(m_i-m_{\min})}\,(c+t-t_i)^{-p}\,, \quad (7)$$

where μ is a constant background rate, K_0 is a constant and $m_{\min}$ is a minimum considered magnitude [*Ogata*, 1988].

[14] We assume a minimum and maximum magnitude of $m_{\min} = 3$ and $m_{\max} = 9$ for our forward simulations and a doubly truncated Gutenberg-Richter law for the magnitude distribution with a standard b value of 1.

[15] To avoid complications by incorrect earthquake classifications, we ignore the spatial component of the triggering process and thus account for all foreshocks and aftershocks independently of their distance to the main shock. For event simulations in time span of 1 year, we use the Monte-Carlo method. To determine one cluster, which consists of one simulated earthquake sequence, we use the following steps:

[16] 1. setting the first event of the simulated sequence to have a zero time and a magnitude randomly selected from the Gutenberg-Richter distribution;

[17] 2. performing a Monte-Carlo simulation of triggered activity initiated by the first event within T;

[18] 3. removing all events with magnitudes less than cut-off magnitude $m_c = 5$ (unobserved seismicity);

[19] 4. defining the event with the maximum magnitude in the sequence as the main shock;

[20] 5. classifying foreshocks as all events before and aftershocks as all events after this main shock.

[21] The described procedure is applied to each simulated sequence. Note that the definition of main shock, foreshocks, and aftershocks is identical to that for the observational data set. However, each synthetic sequence is only related to correlated events containing no independent background activity. Thus, our synthetic simulations correspond to the result of a perfect cluster selection procedure. In most simulations, the initial event is small and no events are simulated above m_c, but we typically simulated 10^8 sequences for each parameter set, leading to a sufficient statistics for main shocks in the analyzed magnitude range $m_c < m_m < m_{\max}$. Note that for simplicity, the duration of the total cluster was chosen to be $T = 1$ year. Thus, the time period for aftershock selection can be smaller than T. However, because the majority of clusters has no or only a very short foreshock sequence, this is not crucial. We checked the results of ETAS simulations for a time window of $T = 2$ years to be sure that the results are stable.

[22] For our simulations, the parameters of the Omori-Utsu law are set to some typical values, namely $c = 0.001$ days and $p = 1.2$. However, we find that the results do not depend significantly on this particular choice. In contrast, the productivity parameters K_0 and α are not directly fixed. Due to the large observational uncertainties and its impact regarding the Båth's law, we explore different values of α in the range between 0.5 and 1.1. The best fit of the simulated data to the observed one in the case of the Bath's law corresponds to $\alpha = 0.95$. Hereinafter, we use $\alpha = 0.95$ for all ETAS simulations presented in this paper. Finally, for given parameters c, p, and α, we determine K_0 indirectly by setting the branching ratio r to a reasonable value.

[23] One can describe the aftershock triggering as a branching process, where each mother event has its own "branch" of aftershocks (every event has only one precursor). The branching ratio r shows the average fraction of triggered events, which is the average number of daughter events per precursor event, and can be calculated by [*Helmstetter et al.*, 2005]

$$r = \int_{m_{\min}}^{m_{\max}} \mathrm{pdf}(m) N_a(m) \mathrm{d}m, \quad (8)$$

where pdf(m) is the probability density function of the earthquake magnitudes, which in the case of the doubly truncated Gutenberg-Richter distribution becomes

$$\mathrm{pdf}(m) = \frac{\ln(10)\, b}{1 - 10^{-b(m_{\max}-m_{\min})}}\, 10^{-b(m-m_{\min})}\,. \quad (9)$$

Furthermore, $N_a(m)$ is the average number of direct aftershocks triggered by an event of magnitude m

$$N_a(m) = K_0 10^{\alpha(m-m_{\min})} \int_0^{\infty} (c+t-t_i)^{-p} \mathrm{d}t = \frac{K_0 10^{\alpha(m-m_{\min})} c^{1-p}}{p-1} \quad (p>1)\,. \quad (10)$$

Consequently, the branching ratio is related to the model parameters according to

$$r = K_0 \frac{c^{1-p}}{p-1} \frac{b}{b-\alpha} \frac{1 - 10^{(\alpha-b)(m_{\max}-m_{\min})}}{1 - 10^{-b(m_{\max}-m_{\min})}} \quad (11)$$

Depending on the value of the branching ratio, it is possible to separate significantly different cases of model behavior: a branching ratio of $r > 1$ leads to exploding seismic sequences; $0 < r < 1$ describes a stationary regime with decaying aftershock sequences; while $r = 0$ implies that all events are independent and thus represents a Poisson process. The first case ($r > 1$) does not have any long-term observational evidence and the branching ratio value has a range $r \simeq 0.5 - 0.8$ according to observations [*Sornette and Werner*, 2005a; *Shearer*, 2012]. This range of values is also used to set K_0 in our forward simulations.

2.3. Restricted ETAS Simulations

[24] In the case of the restricted ETAS simulations, we use constraints for the aftershock productivity based on the hypothesis of static stress triggering. For this purpose, we exploit the results of [*Hainzl et al.*, 2010], who analyzed a simple clock-advance model. The model assumes that the total number of triggered events N_a in response to a Coulomb stress change ΔCFS is equal to the number of events which would have been triggered as independent events by an equivalent tectonic stress loading during a much longer time interval. In this case, the number of triggered aftershocks can be shown to be

$$N_a = \frac{V}{\langle M \rangle} \Delta \mathrm{CFS}, \quad (12)$$

where V is a seismogenic volume and $\langle M \rangle$ is the average long-term seismic moment release per earthquake. The latter

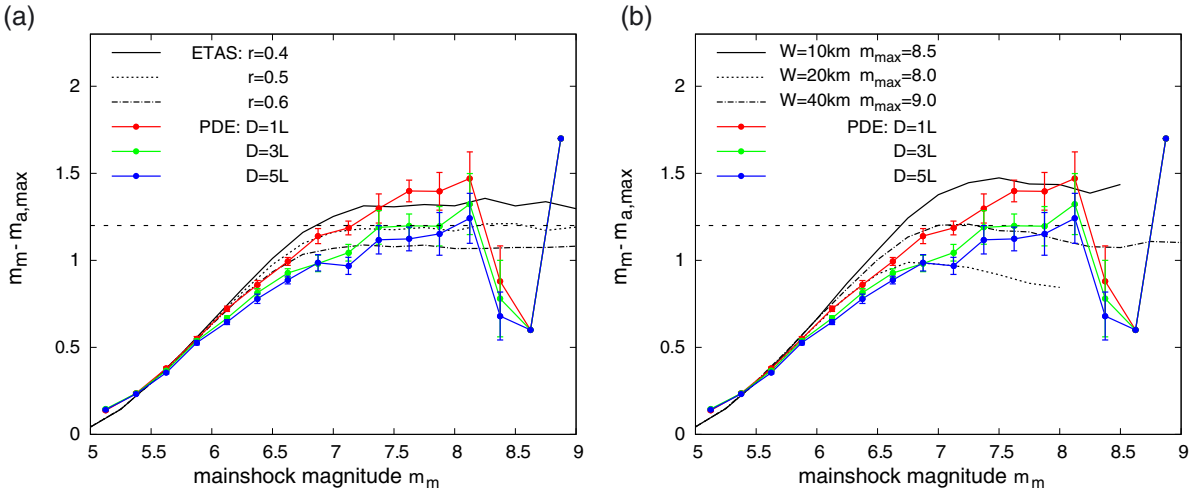

Figure 3. (a, b) The mean value of the magnitude difference between the main shock and its largest aftershock for sequences with at least one aftershock. The observed values (colored dots) for different spatial selection windows according to [*Tahir et al.*, 2012] are compared to ETAS simulations ($m_{\min} = 3, m_{\max} = 9, m_c = 5, b = 1.0, c = 0.001$ days, $p = 1.2, \alpha = 0.95$) (black lines). In Figure 3a, the aftershock productivity scales with $K_0 10^{\alpha m}$ and K_0 are calculated from the branching parameter r. In contrast, in Figure 3b, the productivity is restricted by the results of [*Hainzl et al.*, 2010]. The set of parameters (W = 10 km, $m_{\max}$ = 8.5) corresponds to the strike-slip regime; (W = 20 km, $m_{\max}$ = 8.0) - normal; (W = 40 km, $m_{\max}$ = 9.0) - reverse.

is related to the magnitude distribution (equation (9)) and can be calculated using the following formula

$$\langle M \rangle \equiv 10^{9.1+1.5 m_{\min}} \frac{b}{1.5-b} \frac{10^{(1.5-b)(m_{\max}-m_{\min})}-1}{1-10^{-b(m_{\max}-m_{\min})}} \text{ [Nm]}. \quad (13)$$

[25] The spatial distribution of ΔCFS depends on the rupture size and thus on the earthquake magnitude. However, the seismogenic depth D_{seis} interval, in which aftershocks can nucleate, is limited. This limitation of the seismogenic zone affects the trigger potential of large earthquakes and leads to a break of the scaling properties. According to numerical results of *Hainzl et al.* [2010], the crossover magnitude m^* can be approximated by

$$m^* = \frac{(\log_{10}(W/4)^2 + 3.49)}{0.91}, \quad (14)$$

where $W = D_{\text{seis}}/\sin(\text{dip})$ is the maximum rupture width of earthquake ruptures in the seismogenic zone for a given dip angle. This magnitude value separates approximately following two cases [*Hainzl et al.*, 2010]:

[26] 1. $m < m^*$ - a main shock magnitude is less than m^*. All significant stress changes typically occur within the seismogenic zone and the aftershock number scales according to

$$N_a(m) = 2\frac{M(m)}{\langle M \rangle} = 2\frac{10^{9.1+1.5m}}{\langle M \rangle} \quad (15)$$

[27] 2. $m \geq m^*$ - a main shock with a magnitude larger or equal to m^*. Parts of significant stress changes occur outside the seismogenic volume and leads to

$$N_a(m) = N_a(m^*) 10^{1.07(m-m^*)}, \quad (16)$$

where $N_a(m^*)$ is given by equation (15).

[28] These forecasts of the static stress-triggering model are now implemented in the ETAS model leading to the so-called restricted model version (RETAS). In particular, the function $g(m) = K_0 10^{\alpha(m-m_{\min})}$ in equation (7) is now replaced by $N_a(m)/\int_0^\infty (c+t-t_i)^{-p} dt$, while all other simulation parameters ($c, p, b, m_{\min}, m_{\max}, m_c$) remain the same. As a result we have the following equation for the RETAS model:

$$\lambda_R(t) = \mu + \sum_{i:t_i<t} \frac{N_a(m)}{\int_0^\infty (c+t-t_i)^{-p} dt} (c+t-t_i)^{-p} \quad (17)$$

where $N_a(m)$ is substituted depending on the event magnitude, with one of the formulas (15) and (16), respectively.

[29] The model directly depends on the maximum rupture width W or alternatively on the width of the seismogenic depth layer D_{seis} and the dip. However, the results also depend significantly on $m_{\max}$ via $\langle M \rangle$. Thus, to explore the dependence, we perform simulations with the RETAS model with three different parameter sets, roughly representing the three types of a focal mechanism: (W = 10 km, $m_{\max}$ = 8.5) - strike-slip; (W = 20 km, $m_{\max}$ = 8.0) - normal; (W = 40 km, $m_{\max}$ = 9.0) - reverse.

3. Results

3.1. Båth's Law

[30] The Båth's law states that the magnitude of the largest aftershock is approximately 1.2 magnitudes less than that of the main shock. In Figure 3, we present the magnitude difference between the main shock and the largest aftershock of the sequence as a function of a main shock magnitude. The straight dashed black line corresponds to the Båth's law ($m_m - m_{a,\max} = 1.2$), while the results for the real catalog are shown by colored lines for different spatial cluster

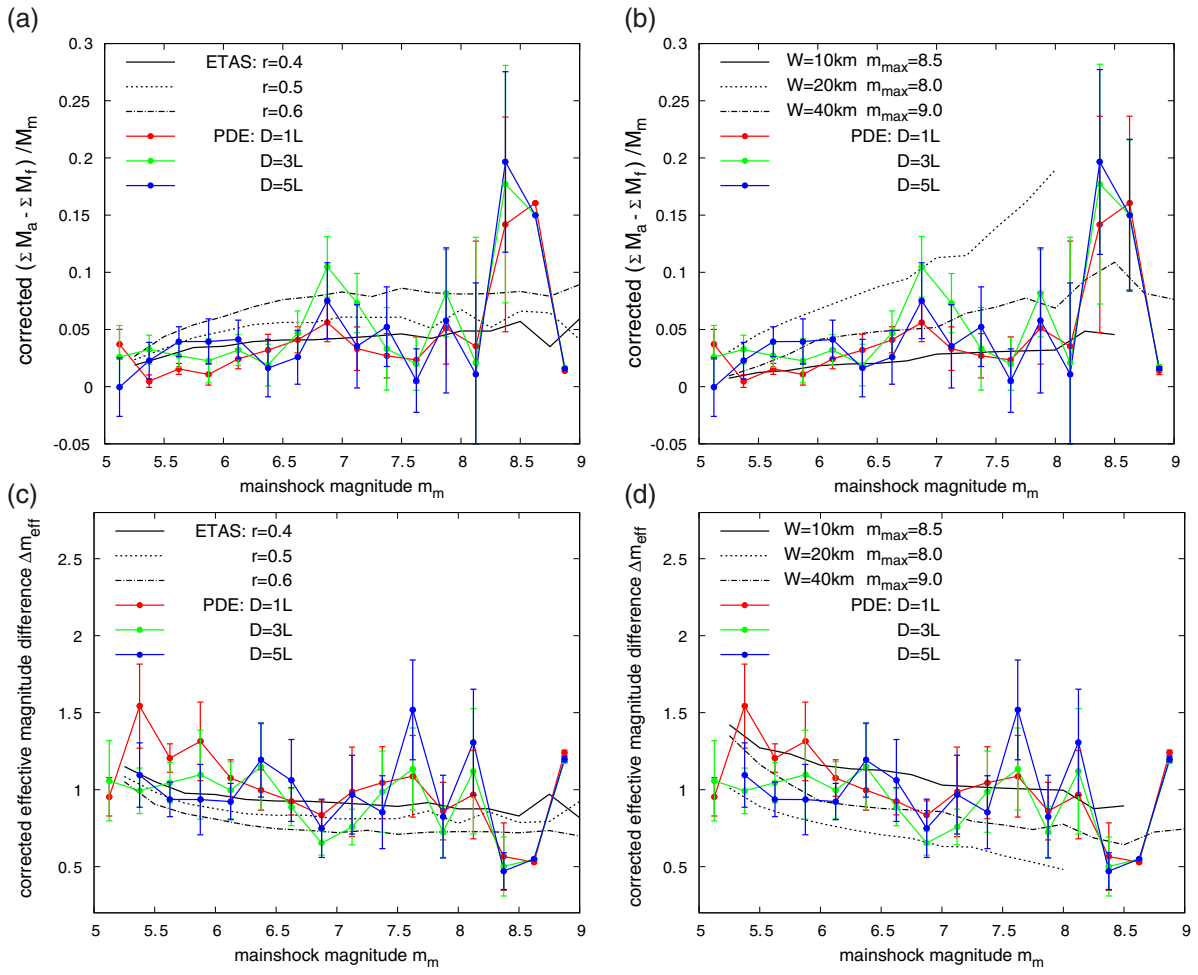

Figure 4. (a, b) The average corrected seismic moment ratio $R_{\mathrm{corr}}(m)$ and (c, d) effective magnitude difference Δm_{eff} as a function of the main shock magnitude. For the description of the symbols and lines, see Figure 3.

selection windows. They are the same for the Figures 3a and 3b, where the observations are compared to the results of the synthetic simulations of the standard and the restricted ETAS model, respectively. Note that in the case of the standard ETAS model, the α value and the branching ratio r have been used as free parameters to optimize the fit to the observations because of the lack of physical constraints. This leads to an α value of 0.95 which is close to $b = 1$ and branching ratios between 0.4 and 0.6. In contrast, the restricted ETAS model (Figure 3b) depends only on the maximum width W of ruptures in the seismogenic zone and the maximum possible magnitude m_{max}. Thus, the observations can be compared to simulations for reasonable values for different focal mechanisms.

[31] Our analysis clearly demonstrates that the Båth's law can only be examined in a small magnitude range. In particular, stable results for the Båth's law can only be found in a repetition between 7 and 8 for the PDE catalog (see Figure 3). This can be explained by the absence of sufficient statistical data for events with magnitudes larger than 8. Here the results for the synthetic catalog are less affected, because the number of simulated sequences can be increased to get stable results. The deviations of the curves for $m_m < 7$ are, on the other hand, the result of the fact that Δm cannot account for main shocks that did not trigger any $m \geq m_c$ aftershock, because in this case the corresponding value is undefined. Thus, Δm is the result of averaging only over sequences with $m_{a,\mathrm{max}} \geq m_c$ and consequently $\Delta m \to 0$ for $m_m \to m_c$.

[32] Furthermore, the results for the observational data are biased by the cluster selection rules. In contrast, we have no problems in the case of our simulations to properly select the dependent events, because we have, by construction, all triggered events above m_c in the catalogs without contamination with independent background events. Moreover, ETAS simulations do not have any spatial component, which could influence the cluster selection. In the present work, we use only the information about magnitude and time of the events of a synthetic catalog. This is not the case for the PDE catalog analysis, and the results are found to depend significantly on the selection parameters. Only a spatial selection window of $D = 3L$ gives a result close to 1.2 Δm, while the value is around 1.4 for $D = L$ and 1.1 for $D = 5L$ (see Figure 3). Increasing of spatial windows leads not only to the larger number of distant aftershocks, but also for more and more independent events. Thus, Δm will decrease necessarily toward 0 for $D \to \infty$. Vice versa, a significant number of

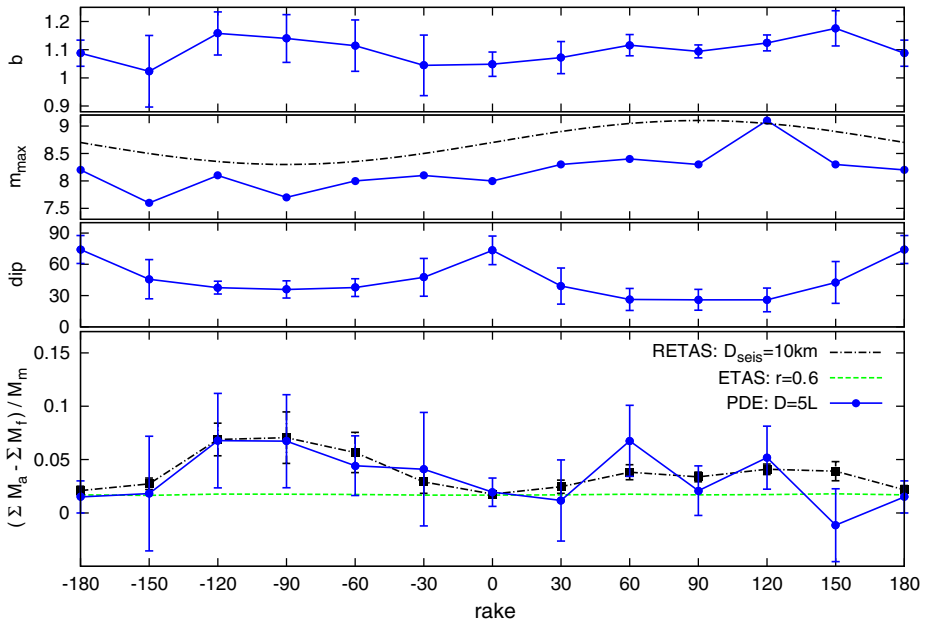

Figure 5. Dependence of b value, m_{max}, dip, and the seismic moment ratio on the rake of the main shock. The black line in the bottom figure refers to the results of restricted ETAS simulations based on *Hainzl et al.* [2010], where m^* is calculated from the dip value and the assumed seismogenic depth D_{seis} according to $W = D_{seis}/\sin(\text{dip})$, and average long-term seismic moment release $\langle M \rangle$ is calculated based on the estimated b value and m_{max} for each rake value. Because the observed maximum magnitudes are only a lower limit of the true value, we used a smoothed and shifted m_{max} curve (black line). The values for the observational data are represented by blue dots. The green dashed line shows the result of standard ETAS simulations with the b value as an input parameter (calculated for the case $D = 5L$) according to the rake of the main shock.

aftershocks is missed for too small selection windows leading to an overestimation of Δm. Due to this interplay, an intermediate value of D has to be chosen, but anyway, the choice remains arbitrary.

[33] To show in which range observational data has larger uncertainties, we calculated the standard deviation of all values of interest. For simulations we do not present any error estimation, because the result of the ETAS model is stable for a large number of simulations. The error estimation for the data was made using a bootstrap method with a Monte-Carlo procedure for data resampling. As events in the catalog are dependent (the magnitude and time of event determine its membership in the cluster), we apply a suitable resampling procedure—random sampling with replacement—by bootstrapping the earthquake clusters used for analysis. In the case of N clusters, we take randomly the same number of clusters from the subset of aftershock sequences using Monte-Carlo method. The random selection gives the replication of about 37% of original points. As a result, we estimate the errors (standard deviation), which take into account the epistemic uncertainty related to a lack of data. Figure 3 presents plus/minus one standard deviation of the magnitude difference in the all magnitude range. Error bars are reliable for $m_m \leq 8$; for the magnitudes $m_m > 8$ the standard deviation cannot be estimated correctly using bootstrap method, because too few observations are available for this range. The largest standard deviation for Δm is around 0.22.

[34] The ETAS model result closest to the Båth's law corresponds to a branching ratio 0.5 and $\alpha = 0.95$. For other α values, Δm is slightly increasing ($\alpha < 0.95$) or decreasing ($\alpha > 0.95$) with increasing main shock magnitudes above 7. For a higher branching ratio $r = 0.6$, Δm is underestimated, and for a smaller one $r = 0.4$, it is overestimated. In contrast, the RETAS simulations do not depend on α and r. However, Figure 3b shows that also in this case of limited degrees of freedom, the results are in good agreement with the observations. The worst fit is observed for the "normal" fault type set of parameters ($W = 20$ km and $m_{max} = 8.0$), however, normal fault main shocks are the smallest sample in the PDE catalog above magnitude 7. In spite of the limitations, all simulations within the physical reasonable range show a rather good correspondence with the Båth's law and the observed data.

3.2. Seismic Moment Ratio R and Effective Magnitude Difference Δm_{eff}

[35] The magnitude range which can be analyzed is significantly larger in the case of the seismic moment ratio $R_{corr}(m)$ and the effective magnitude difference Δm_{eff}. This becomes clear in Figure 4, where the results for the simulations of the ETAS and RETAS models are compared to the results of the PDE catalog. The reason is that also main shocks with no aftershocks above m_c are taken into account. In these cases, the seismic moment of the aftershocks is zero. Furthermore, the cluster selection criteria are less critical, because subtracting the seismic moment released in the preceding time window, M_f, avoids a systematic effect of the included background activity. In fact, the results for the three different spatial windows show no systematic trend for the PDE catalog. Quite large fluctuations for the observed data are likely

related to the relative small amount of main shocks in the magnitude bins.

[36] The comparison of the observed values with the synthetic data shows that both ETAS and RETAS reproduce the observations within one error interval. Overall, the RETAS model with less degrees of freedom can reproduce the general trend of the observed data even better, particularly in the case of the effective magnitude difference Δm_{eff} (Figure 4d). The values of Δm_{eff} are significantly smaller than Δm and range between 0.7 and 1, with a slight negative trend for increasing main shock magnitudes.

[37] Errors estimated for corrected seismic moment ratio R_{corr} and Δm_{eff} give one more indirect confirmation that these values can be analyzed in a wide range of magnitudes. For Figures 4a and 4b, the standard deviation of R_{corr} is only slightly increasing up to magnitude 8, which shows that results are equally reliable. For Figures 4c and 4d, errors are approximately in the same range for all magnitudes ($m_m \leq 8$). On average, errors are larger than in the case of the Båth's law (see Figure 3), but remain smaller than ± 0.32.

3.3. Dependence on the Focal Mechanism

[38] We analyze the sequence characteristics as a function of the rake of the main shocks similar to the work of Tahir (M. Tahir and J.-R. Grasso, Faulting style controls on the Omori law parameters from global earthquake catalogs, submitted to *Journal of Geophysical Research*, 2012). For this purpose, we evaluate the parameters in bins of 30°. It is found that the focal mechanisms have some obvious correlations with parameters such as the b value, $m_{\max}$ (the maximum magnitude observed in the specific rake range), dip and seismic moment released by aftershock sequences (see Figure 5).

[39] The standard ETAS model depends only on the b value, on the contrary, the RETAS model explicitly depends on the dip, b, and $m_{\max}$. The observed b value is found to be unable to explain the variations of the R ratio of the real data in the case of a standard ETAS model (see the green curve in Figure 5). We therefore compare the observed variation of R with the R values forecasted by the RETAS model based on the observed dip, b, and $m_{\max}$ values in each rake bin. Specifically, we use the dip, b, and $m_{\max}$ values as input to calculate m^* and $\langle M \rangle$ and run 10^8 simulations to get the average seismic moment ratio for a given rake bin. We find that the RETAS model is overall in agreement within error bars with the observed data. For fitting, we used a depth of the seismogenic zone of $D_{\text{seis}} = 10$ km. Smaller or larger values would lead to a scaling of the resulting curve to smaller or larger R values, respectively. The errors shown in Figure 5 for the RETAS model are smaller than for the observational data, because they are only related to the uncertainties of the b and dip input values.

[40] The seismic moment released by aftershock activity is proportional to the number of events in the post-main shock sequence. On its turn, the number of aftershocks (equation (12)) is controlled by two factors: the maximum rupture width W and the average seismic moment per earthquake which depends on b value and the maximum magnitude. In response to these dependencies, the seismic moment ratio has a tendency to be the largest in the case of normal, intermediate for thrust and lowest for strike-slip faulting. This means that the amount of aftershock energy with respect to the main shock magnitude seems to be the largest for normal faulting and the lowest for strike-slip faulting.

4. Discussion

[41] The seismic moment ratio R and the corresponding effective magnitude difference Δm_{eff} (which are based on all clusters, but not only on the subsets with at least one aftershock) are shown to be superior to Δm, because these values are less affected by cluster selection rules and can be analyzed in a significantly larger magnitude range. However, similarly to Δm, these parameters are strongly fluctuating for single aftershock sequences due to the power law distribution of seismic moment release related to the Gutenberg-Richter magnitude distribution. Thus, any forecast of these values for individual forecasts is subject to large uncertainties.

[42] The average properties of a large sample of observed aftershock sequences can yield important insights into the physical processes underlying earthquake triggering. The best ETAS model needs $\alpha \approx b$ and a branching ratio of approximately 0.4 to explain the observations for the global data. Here it is important to emphasize that the branching parameter depends on the minimum earthquake magnitude. For practical reasons, we used in our simulations a minimum magnitude of 3, which is certainly above the true minimum earthquake magnitude m_0 in nature. According to [*Sornette and Werner*, 2005b], the true branching ratio r can be estimated from the value $r(m_{\min})$ obtained for simulations in the magnitude range $[m_{\min}, m_{\max}]$. For the special case $\alpha = b$ it is given by

$$\begin{aligned} r &= r(m_{\min}) \frac{m_{\max} - m_0}{m_{\max} - m_{\min}} \frac{1 - 10^{-b(m_{\max} - m_{\min})}}{1 - 10^{-b(m_{\max} - m_0)}} \\ &\approx r(m_{\min}) \frac{m_{\max} - m_0}{m_{\max} - m_{\min}} \end{aligned} \tag{18}$$

This leads, for example, to a branching ratio of approximately 0.7 for $m_0 = -2$. Vice versa, the limit of $r = 1$ is related to an absolute minimum magnitude of about $m_0 = -6$.

[43] This extrapolation implies a scale invariance of the trigger potential. However, we have shown in the last section that the RETAS model with a break of the scaling properties leads to similar or even better results. Additionally, the RETAS model can explain the observed dependence on the focal mechanism of the main shock (rake-dependence). Thus, the good agreement between the RETAS model and the observations indicates that static stress triggering could work. This would also imply that the trigger potential of small magnitude events is weaker than expected by the ETAS model and, consequently, the overall process is clearly subcritical.

[44] Besides aftershocks, aseismic postseismic deformation is often triggered by main shocks. The aseismic moment release is sometimes several times larger than the aftershock moment. Thus, it might be important to additionally include the aseismic moment release in the analysis of R and Δm_{eff}, which is, in principal, straightforward. However, this is difficult in practice and is left for future work, because

the information related to postseismic deformations are not systematically recorded in earthquake catalogs.

5. Conclusion

[45] The seismic moment released by aftershocks is shown to be an alternative diagnostic tool to characterize aftershock sequences. As demonstrated in the present paper, the seismic moment release ratio and the corresponding value of Δm_{eff} can be analyzed in a much wider range compared to the often used value of Δm, which is related to the magnitude difference between the main shock and its largest aftershock. Our obtained results for global seismicity (PDE world catalog) indicate that the seismic moment released by aftershocks is approximately 5% of the main shocks seismic moment. Furthermore, the seismic moment release seems to be correlated with the focal mechanism, in particular, with the rake of the main shock. Both observations are used to test the agreement with the static stress-triggering hypothesis, which predicts that the total number of aftershocks is directly related to observable parameters such as the seismogenic width and the parameters of the magnitude distribution. Additionally, static stress triggering can explain a break of the aftershock productivity scaling, which is related to the finite width of the seismogenic zone. While the standard ETAS model based on scale-invariant triggering probabilities is found to reproduce the general features quite well, it does not explain the systematic variations with the focal mechanism. Furthermore, the productivity parameters of this model, K_0 and α, are free fitting parameters without any direct physical interpretation. In contrast, the ETAS model constrained by static stress triggering, the so-called RETAS model, is found to reproduce the observations even better, but without free fitting parameters. Our results indicate that the constraints derived from static stress triggering are in agreement with the data, and that these results can be used to constrain the average total seismic moment released by aftershock sequences.

[46] **Acknowledgments.** We acknowledge two anonymous reviewers and the Associate Editor for their helpful comments. Furthermore, we are thankful to Álvaro González and Camilla Cattania for useful discussions. This work was supported by Helmholtz Graduate Research School GeoSim and the Potsdam Research Cluster for Georisk Analysis, Environmental Change, and Sustainability (PROGRESS) project.

References

Båth, M. (1965), Lateral inhomogeneities of the upper mantle, *Tectonophysics*, *2*(6), 483–514.

Console, R., A. M. Lombardi, M. Murru, and D. Rhoades (2003), Båth's law and the self-similarity of earthquakes, *J. Geophys. Res.*, *108*(B2), 2128, doi:10.1029/2001JB001651.

Felzer, K. R., T. W. Becker, R. E. Abercrombie, G. Ekström, and J. R. Rice (2002), Triggering of the 1999 M_w 7.1 Hector Mine earthquake by aftershocks of the 1992 M_w 7.3 Landers earthquake, *J. Geophys. Res.*, *107*(B9), 2190, doi:10.1029/2001JB000911.

Hainzl, S., and D. Marsan (2008), Dependence of the Omori-Utsu law parameters on main shock magnitude: Observations and modeling, *J. Geophys. Res.*, *113*, B10309, doi:10.1029/2007JB005492.

Hainzl, S., G. B. Brietzke, and G. Zoeller (2010), Quantitative earthquake forecasts resulting from static stress-triggering, *J. Geophys. Res.*, *115*, B11311, doi:10.1029/2010JB007473.

Hanks, T. C., and H. Kanamori (1979), A moment-magnitude scale, *J. Geophys. Res.*, *84*, 2348–2350.

Helmstetter, A., and D. Sornette (2003), Båth's law derived from the Gutenberg-Richter law and from aftershock properties, *Geophys. Res. Lett.*, *30*, 2069, doi:10.1029/2003GL018186.

Helmstetter, A., Y. Y. Kagan, and D. D. Jackson (2005), Importance of small earthquakes for stress transfer and earthquake triggering, *J. Geophys. Res.*, *110*, B05S08, doi:10.1029/2004JB003286.

Ogata, Y. (1988), Statistical models of point occurrences and residual analysis for point processes, *J. Am. Stat. Assoc.*, *83*, 9–27.

Shearer, P. M. (2012), Self-similar earthquake triggering, Båth's law, and foreshock/aftershock magnitudes: Simulations, theory, and results for southern California, *J. Geophys. Res.*, *117*, B03610, doi:10.1029/2011JB008957.

Sornette, D., and M. J. Werner (2005a), Constraints on the size of the smallest triggering earthquake from the epidemic-type aftershock sequence model, Båth's law, and observed aftershock sequences, *J. Geophys. Res.*, *110*, B08304, doi:10.1029/2004JB003535.

Sornette, D. D., and M. J. Werner (2005b), Apparent clustering and apparent background earthquakes biased by undetected seismicity, *J. Geophys. Res.*, *110*, B09303, doi:10.1029/2005JB003621.

Stein, R. S. (1999), The role of stress transfer in earthquake occurrence, *Nature*, *402*, 605–609.

Tahir, M., J.-R. Grasso, and D. Amorèse (2012), The largest aftershock: How strong, how far away, how delayed?, *Geophys. Res. Lett.*, *39*, L04301, doi:10.1029/2011GL050604.

Utsu, T., Y. Ogata, and R. S. Matsu'ura (1995), The centenary of the Omori formula for a decay law of aftershock activity, *J. Phys. Earth*, *43*, 1–33.

van Stiphout, T., J. Zhuang, and D. Marsan (2012), Seismicity declustering, *Community Online Resource for Statistical Seismicity Analysis*, doi:10.5078/corssa-52382934, Available at http://www.corssa.org.

Wells, D. L., and K. J. Coppersmith (1994), New empirical relationships among magnitude, rupture length, rupture width, rupture area, and surface displacement, *Bull. Seismol. Soc. Am.*, *84*, 974–1002.

Zhuang, J., D. Harte, M. J. Werner, S. Hainzl, and S. Zhou (2012), Basic models of seismicity: Temporal models, *Community Online Resource for Statistical Seismicity Analysis*, doi:10.5078/corssa-79905851 [Available at http://www.corssa.org.]